Aerospace Science and Technology 162 (2025) 110172

Contents lists available at ScienceDirect

Aerospace Science and Technology

journal homepage: www.elsevier.com/locate/aescte

Experimental and numerical investigation of a novel strut-mounted roller-screw inerter for helicopter vibration attenuation

Aykut Tamer [a,*], Pierangelo Masarati [b], Michele Zilletti [c], Luigi Bottasso [c]

[a] University of Bath, Claverton Down, Bath, BA2 7AY, UK
[b] Politecnico Di Milano, Via La Masa 34, Milan, 20156, Italy
[c] Leonardo Helicopters, Via Giovanni Agusta 520, Samarate, VA, 21017, Italy

ARTICLE INFO

Communicated by Cummings Russell

Keywords:
Helicopter vibration isolation
Mechanical inerter

ABSTRACT

A prominent problem of helicopters is the high vibrational levels due to the high-amplitude excitation forces originating from the main rotor. The ideal solution to reduce vibrations transmitted through the struts is to isolate the fuselage from the main rotor excitation at gearbox struts; therefore the overall vibration attenuation is achieved rather than local solutions. However, the limited available volume around the struts limits the application of existing vibration dampers. To solve the challenge, this work proposes a novel vibration attenuation idea that can effectively perform in confined spaces. Based on the inerter concept of roller-screw type, the axisymmetric design encloses the strut and shares its attachment points, providing a compact solution. The concept is demonstrated through experiments to identify realistic characteristics and rigorous numerical analysis using lumped-parameters and high-fidelity aeroelastic helicopter models to demonstrate vibration mitigation. The results show that the non-linear effects due to friction reduce the effectiveness at low excitation amplitudes; however, satisfactory vibration attenuation levels are achievable at high vibratory loads, a more critical condition for vibration alleviation performance.

1. Introduction

1.1. Helicopter vibrations

Vibrations in helicopters mainly originate from the periodic interaction of the main rotor blades with their edgewise aerodynamic field. They may severely impact practical performances and comfort, even reducing the theoretical maximum achievable speed [1,2]. Increased maintenance cost is another consequence, as the likelihood of structural failures increases with high-frequency, high-amplitude excitation [3]. Moreover, severe vibration levels can even cause loss of control due to involuntary interaction and control loop closure with the pilot [4]. Finally, vibrations may lead to physiological and psychological reactions in the human body [5,6], which are felt by pilots, cabin crew, and passengers of the helicopter, resulting in discomfort [7] and reduced human performance [8].

The dominant sources of vibratory excitation in helicopters are the forces and moments originating from the rotors, fuselage aerodynamics, engines, and transmission. Although all these sources contribute to the vibratory level, the predominant loads of the conventional main+tail rotor helicopter configuration originate from the main rotor. In a well-maintained helicopter, balanced rotors act as a filter that effectively cancels vibrations at several multiples of the rotor's fundamental frequency that originate from the periodicity of the excitation in steady flight conditions, contributing to a smoother ride. However, even in perfectly balanced rotors, vibratory loads at integer multiples of the rotor's fundamental frequency, namely its angular velocity Ω times the number of blades N ($N\Omega$, or N/rev in non-dimensional form) are transmitted to the airframe [9]. These are indicated as iN/rev loads, with $i \in \mathbb{N}^+$. Forces and moments corresponding to $i = 1$, the fundamental harmonic of the excitation, dominate over those at higher multiples; hence, they are considered the main driver when addressing vibration reduction.

1.2. Vibration reduction in helicopters

Achieving a smooth-ride helicopter is challenging and requires several strategies during design. Although in principle the generation of vibratory loads can be reduced if not minimized by using advanced simulation tools for their prediction in the design phase [10,11], residual vibrations are unavoidable. The resulting vibratory levels are usually

* Corresponding author.
E-mail address: at2849@bath.ac.uk (A. Tamer).

https://doi.org/10.1016/j.ast.2025.110172
Received 16 January 2025; Received in revised form 17 March 2025; Accepted 26 March 2025

Available online 31 March 2025

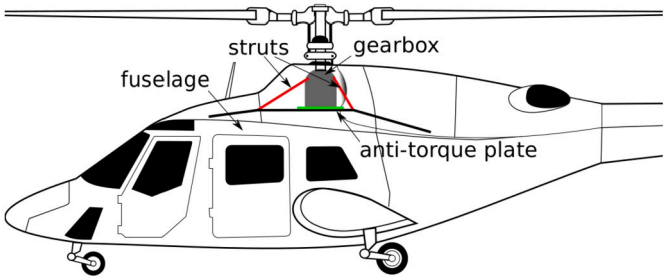

Fig. 1. Main rotor gearbox struts and their typical connection points.

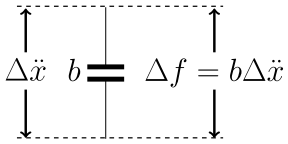

Fig. 2. The inerter produces an internal force proportional (and opposite) to the relative acceleration.

high enough to require the implementation of vibration attenuation devices. For this reason, vibration reduction using alternators and isolators is still a standard practice in the rotorcraft industry [1] and they can achieve substantial reductions [12].

Several vibration reduction techniques and devices have been tested on helicopters [13]. Among those, a broadly used approach consists of implementing active and passive vibration attenuation devices mounted in parallel to or in series with the struts that support the main rotor gearbox, as illustrated in Fig. 1. The struts, usually four, represent the main load path for forces transmitted from the main rotor to the fuselage, being the torque usually carried by other structural elements. Therefore, they provide global isolation of the airframe from the excitation caused by the main rotor.

Strut-mounted devices can be active or passive. The active solutions can alleviate vibrations in a broad range of frequencies; however, the external power requirement and the additional equipment needed to run them (computers, actuators, etc.) can make them less appealing. Considering that the rotor already filters vibrations other than the multiples of the blade passing frequency, tonal vibration attenuation near N/rev can be sufficient in most cases. For this reason, passive devices are commonly used to isolate the cabin from the main rotor.

A typical solution implemented at the struts is the DAVI (Dynamic Anti-resonant Vibration Isolator), a mass on a lever mounted in parallel to the gearbox suspension [14,15]. The ARIS (Anti-Resonance Isolation System) is another type of isolator device; mechanical and hydraulic versions have been proposed [16]. Similar to the previous one is the SARIB (*Suspension Anti-Résonante Intégrée à Barres*, or anti-resonance suspension integrated with the struts) [17], whose tuning mass is in series with the gearbox suspension. A different technique consists of accelerating a low-viscosity fluid between two chambers, letting the pressure differential caused by the fluid's inertia loads resulting from the relative motion counteract the vibratory load [18–20].

1.3. Inerter

An alternative mechanical device designed for vibration alleviation is the *inerter*. An inerter creates an internal force in response to a relative acceleration of its terminals, as illustrated in Fig. 2, as opposed to a conventional tuned mass damper, whose reaction force is proportional to its absolute acceleration in the inertial reference frame.

Inerters are analogous to capacitors in an electric circuit; to a certain extent, they can be considered the "missing" mechanical element in the analogy between electric and mechanical systems [21]. Since the late 2000s, various mechanical inerters have been designed based on rack-and-pinion and screw mechanisms [22–24], in addition to designs that utilize the inertia of a liquid [25,26] (Fig. 3). Both types of mechanical inerters rely on amplifying linear motion by converting it into rotational motion of a spinning mass, which generates an inertial force.

The rack and pinion type inerter consists of a rack and a pinion mechanism. When an external force moves the rack linearly, the pinion rotates, transferring motion to a high-inertia flywheel or mass via a gear system (Fig. 3a).

The screw-type inerter consists of a lead screw and a nut containing ball bearings. When an external force moves the screw linearly, the nut rotates and transfers motion to flywheel (the tuning inertia) attached on screw (Fig. 3b).

The fluid type inerter, on the other hand, accelerates a fluid mass between two chambers, creating a pressure difference on the two surfaces to which the two terminals are connected to (Fig. 3c).

Irrespective of the mechanism used, the resulting forced response is proportional to an inertial constant, b, and the relative acceleration between its ends, $\Delta\ddot{x}$, namely

$$\Delta f = b\Delta\ddot{x} \tag{1}$$

acting opposite to the relative acceleration. The inertance (b, an equivalent inertia) depends on the type of inerter and its internal kinematics.

Inerter-based solutions have recently been studied to suppress vibrations in structures for harmonic [27,28] and random excitations [29,30] and to improve seismic performances of buildings [31,32]. These studies showed that inerter-based vibration suppression devices perform better than the classical tuned mass dampers. While the results are promising, non-linearities such as damping, backlash, parasitic mass and stiffness should not be ignored in an inerter device. For instance, Smith and Wagg in [33] showed through experiments that friction dominated the force produced by a fluid inerter. Similarly, De Domenico et al. in [34] reported that an inerter-damper is a more accurate model compared to an inertia-only behaviour. Losses can also be frequency-dependent due to significant hysteresis damping in some designs, as reported by Deastra et al. [35].

1.4. State of the art

To investigate the concept for helicopter vibration attenuation, a roller-screw type inerter was suggested. The inerters are intended to be mounted in parallel with the main gearbox struts to reduce the vibratory load transmitted to the fuselage. Roller screws are better suited than other mechanical inerter types (compared to rack-pinion and ball-screw), especially due to high-load capacity, low friction and low screw leads [36]. These aspects better suit helicopters for the reasons illustrated below:

- High load capacity: the vibratory loads transferred through the struts are high enough to cause significant vibrations in the cabin. The device should withstand high dynamic loads to operate on a helicopter strut.
- Low friction: among screw mechanisms, roller screws show the least level of friction. Low friction reduces dissipation in the system, therefore producing better vibration attenuation.
- Low screw lead: screw lead directly affects the amplification of rotation speed, which increases the amplitude of the force generated by the inerter. Roller screws can reach much lower screw leads compared to ball screws, therefore higher counteracting force levels can be achieved.
- Symmetric and compact structure: the available volume is limited near the gearbox area, usually enclosed by a streamlined cowling to reduce aerodynamic drag. Therefore, the strut-mounted device should be of compact design and possibly enclose the strut to use less volume, instead of being mounted at its side. Roller screws are symmetric cylindrical devices that can enclose the strut in a dedicated design.

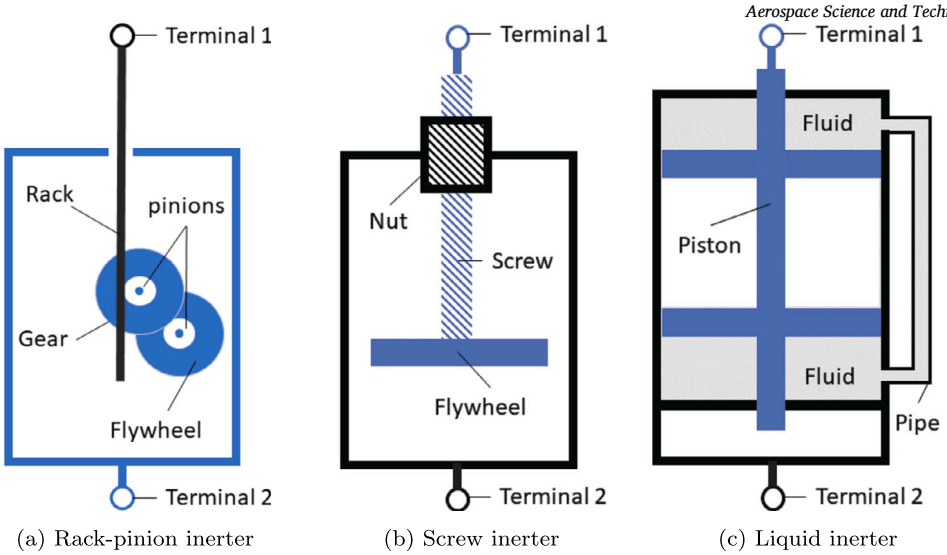

Fig. 3. Inerter types described in literature.

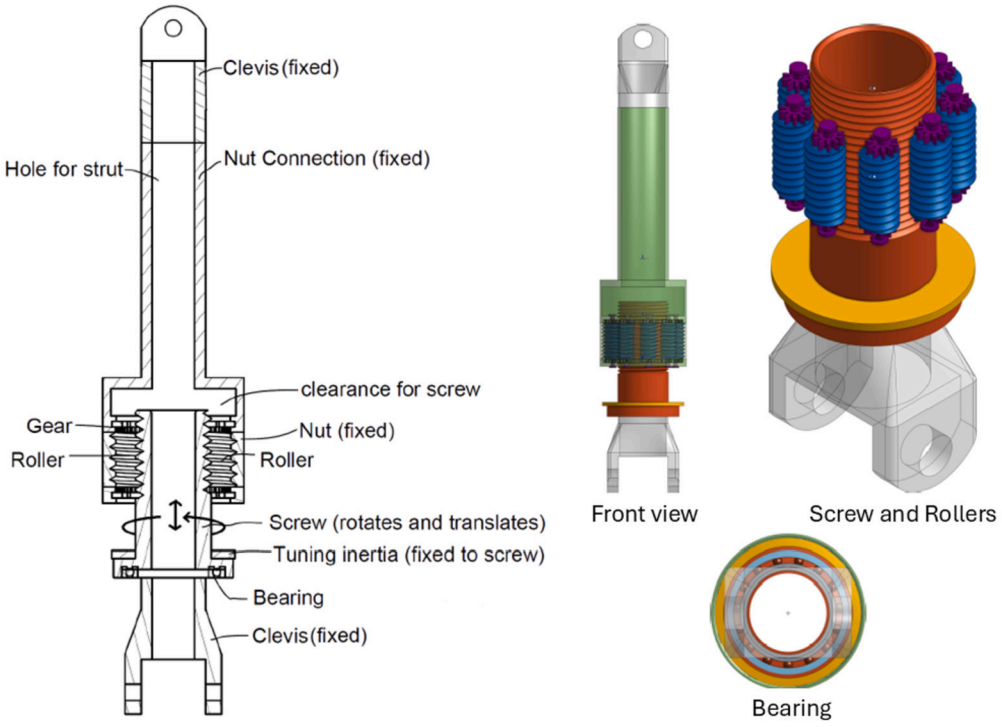

Fig. 4. Strut-mounted roller screw inerter for helicopter vibration attenuation with its components highlighted on a 2D cut out and visualised using a 3D rendered model.

According to the above advantages, a strut-mounted vibration attenuation device has been conceived, designed, and developed based on a roller-screw inerter. The concept has been patented for future use in helicopters [37]. Fig. 4 presents the concept, which works according to the following *modus operandi*:

- the screw end allows the mounting of a bearing;
- a bearing is located between the screw-end and a convenient support element (a fixed clevis for example), where the strut is connected, which allows relative rotation of the screw about its longitudinal axis;
- on the upper side, the nut has an extension (nut connection) that is clamped to the other support (clevis for example), therefore holding the nut fixed;
- the inerter encloses the strut, which requires a hole through the nut, nut connection, screw, and bearing;
- the strut and the inerter ends are mounted to the gearbox and airframe, sharing the pins so that both operate between the same terminals;
- when a relative axial motion is imposed at the two ends, the fixed nut guides the rollers;
- the rollers, which are synchronized using gears, rotate the screw and the attached tuning inertia, therefore converting the motion from linear to rotational;
- a tuning inertia, ideally a high-density material disc is fixed on the screw shaft, which is tuned for a specific frequency to generate a counteracting force proportional to the square of the frequency.

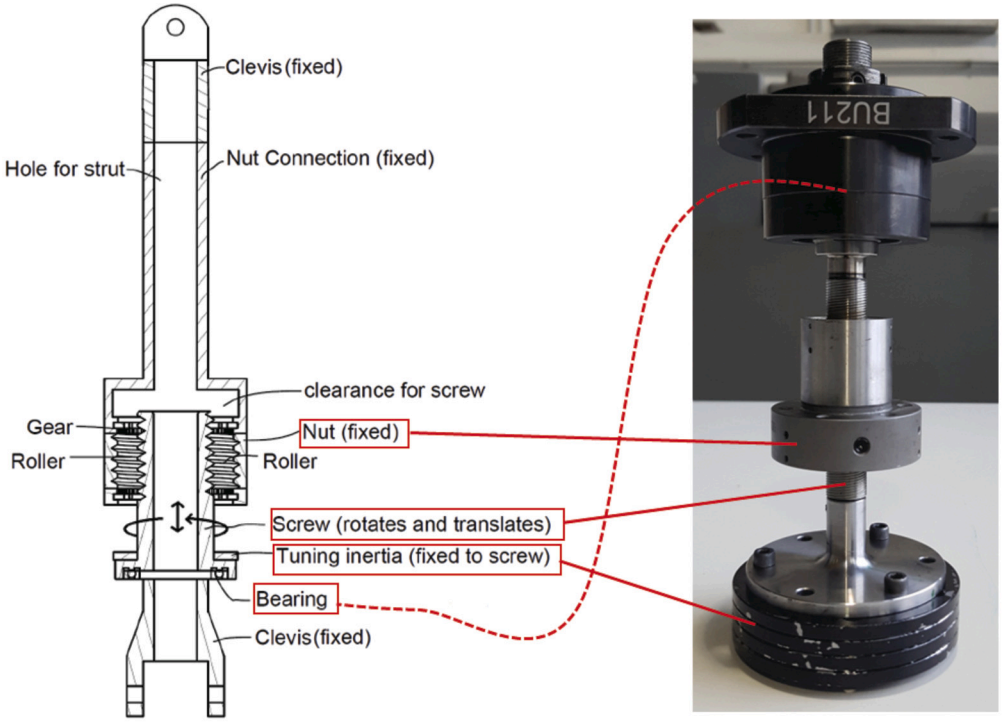

Fig. 5. Proposed inerter for helicopter strut and realisation using Rollvis roller screw actuator converted to inerter using tuning discs and bearing.

The inertance b is the critical parameter to tune the device for the target frequency. Hence, it is worth stating how inertance is calculated for this concept. For a screw-type inerter, the value of the inertance b is related to the total inertia of the rotating mass, $I = I_{\text{disc}} + I_{\text{screw}}$, and screw pitch P [21], which leads to:

$$b = \frac{I}{P^2} \tag{2}$$

where the pitch of the screw (P) is defined as the axial displacement resulting from a 2π rad rotation. In this proposed solution, the inertance should be tuned to the lowest excitation frequency, which is N/rev or, in dimensional terms, $\omega = N\Omega$. Considering that the strut applies a restoring force proportional to its stiffness k, the tuning inertance required to isolate the lower terminal from an excitation at the upper one is:

$$b = \frac{k}{\omega^2} \implies I = \frac{P^2}{\omega^2} k. \tag{3}$$

This inertance corresponds to the inertia of the tuning mass, which increases with the square of the screw pitch and strut stiffness, while decreasing with the excitation frequency.

1.5. Outline

This work investigates the use of a novel roller-screw inerter for helicopter cabin vibration isolation based on experiments and numerical analysis. It provides a rigorous analysis of the concept introduced by the authors in [38]. In the subsequent Section 2, the experimental verification of the roller-screw inerter concept is presented, and the friction levels expected from the device are identified. In Section 3, an operational model of the device that uses the identified characteristics is applied to a lumped parameter helicopter model first, and then to a detailed model of the structural dynamics of a helicopter. The presented results illustrate the potential benefits of the inerter for cabin vibration attenuation. Section 4 summarizes the key findings of this study and discusses the additional research required to improve the technology readiness level of the proposed concept.

2. Experimental identification

This section presents the experimental activity performed on a roller-screw inerter, to assess whether the device operates as expected. Additionally, this activity supported friction level identification in the device under investigation, to obtain a more realistic model for the subsequent analyses.

2.1. Test set-up

The concept shown in Fig. 4 requires a dedicated design that allows the pass-through of the strut. However, such a cavity to house the strut is not related to the operation of the inerter, rather it is required in the dedicated helicopter application depending on the strut diameter of a target helicopter. Therefore, to demonstrate a proof of concept and assess its fitness for the purpose, an off-the-shelf roller screw was converted into an inerter instead of manufacturing a dedicated device with the required pass-through hole. The tested specimen was based on a custom-made roller screw manufactured by Rollvis [39], with additional features added to turn it into an inerter, namely a bearing to decouple the linear axial motion from the screw rotation and a screw end to mount the tuning-inertias, referring to the same features of Fig. 4, as presented in Fig. 5, therefore ensuring parallelism between the proposed design and the test item.

The roller screw and the additional features were assembled by the manufacturer. In its final form, the inerter test specimen is composed of the screw, nut, bearing, screw-end, and tuning discs. The screw is a partially M5 threaded rod, which rotates with respect to the fixed nut. The nut forms one terminal of the inerter and includes rollers inside to allow the screw to rotate. Flanged holes are used for assembly. The bearing is attached to the screw shaft from the inside. The outer part is fixed and forms the other terminal of the roller screw. The bearing transfers the axial force to the screw without any torsional moment being applied to the screw shaft. In the test set-up, the bearing connects the inerter to the actuator. The screw end is a circular plate pinned to the end of the screw; a set of holes is provided to mount the tuning masses. The tuning masses are steel discs mounted at the end of the screw shaft to change

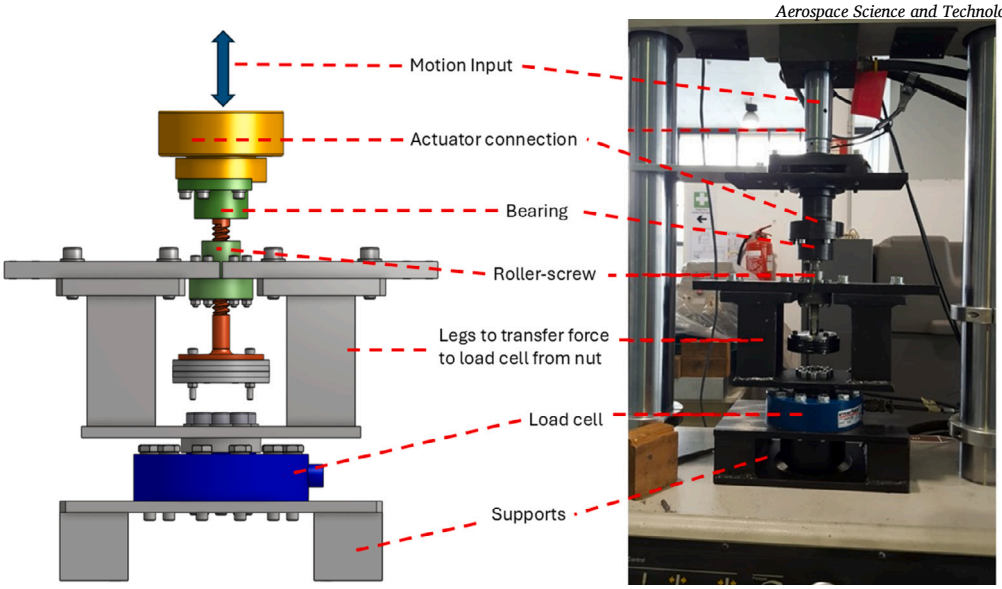

Fig. 6. Test set-up design capable of applying the desired motion input to the bearing and measuring the force on the nut (a), and its realisation on a MTS hydraulic actuator (b).

the inertance of the device. Higher-density material could be used in a practical implementation, should the device's volume be critical.

The inerter must be connected to two terminals, contrary to typical tuned mass dampers having a freely moving tuning mass. In a typical helicopter application, the two terminals are the ends of the strut. A laboratory realization of this arrangement has been achieved by clamping one end to a load cell and connecting the other to an actuator as presented in Fig. 6(a). The benefit is twofold. First, the relative acceleration of the inerter's ends is directly obtained from the actuator controller as the amplitude Δx, whose corresponding acceleration is obtained by multiplication by the negative of the square of the excitation frequency ω. Second, the firmly fixed load cell can provide reliable force data. As a result, the total force output can be related to the actuator displacement for the mechanical identification of the device's characteristic transfer function:

$$f = b\Delta\ddot{x} + f_f \text{ or } f = -\omega^2 b\Delta x + f_f \tag{4}$$

when subjected to harmonic motion of frequency equal to ω, where b is again the total inertance and f_f is the friction force, discussed later in this section.

The bottom side of the load cell was fixed to the frame, while the upper side was connected to the inerter nut. Since the actuator was connected to the bearing, the other terminal, namely the nut, had to be connected to the load cell. To achieve this, a frame was designed, that connected the nut to the inerter while providing space for the tuning discs. An MTS 858 Bionix machine available at Politecnico di Milano was selected as the actuator. The actuator head was connected to the inerter bearing through rigid connections. An Interface 1700 series load cell with a 22 kN limit was used to measure the force output, which completes the rig, as shown in Fig. 6(b).

The frame was sized based on the dimensions of the inerter and aimed to have a first natural frequency much higher than that of typical helicopter N/rev vibration frequencies. The FEM analysis showed a lowest natural frequency of about 110 Hz, whose mode shape is shown in Fig. 7. This value is much higher than the inerter tuning frequency, which is selected within the N/rev frequency range of conventional helicopters — typically between 10 Hz and 30 Hz, depending on the size (and thus on the angular velocity, loosely inversely proportional to the rotor radius) and number of blades —, as reported for example in [40].

While the frame itself is safe from resonance, it is only a part of the whole rig and it is assembled to the machine through the load cell and another base structure, all are connected to the ground through rubber supports. Therefore it is also worth checking the natural frequency of the whole assembly, which requires an experimental approach due to the increased complexity. For this purpose, an impact hammer test was conducted to identify the resonance frequencies in the overall test set-up. 10 uni-axial accelerometers aligned in vertical direction were mounted on the structure and the base of the testing machine and the rig was hit, as shown in the left part of Fig. 8. Two normal vibration modes of the test equipment, respectively at about 16 Hz and 22 Hz, were identified as shown in the centre and right of Fig. 8. Both modes show a substantial vertical motion of the base of the test equipment; thus, they are dominated by the rigid-body motion of the whole assembly. As the base of the test equipment could not be modified to overcome this limitation, experimental results above 15 Hz would be misleading, and especially 20 Hz where the unexpected motion of the base dominates the response, would likely be amplified and hence cannot be considered reliable. Nevertheless, 20 Hz is still high enough to refer to typical medium and medium-large helicopter N/rev frequencies and the experiments could provide insight to helicopter application.

2.2. Measurements

The friction characteristics must be identified to improve the correspondence between the theoretical model and the measured loads, and thus obtain realistic models, discussed in detail in Section 3.1, to demonstrate the concept. Additionally, friction is crucial to address existing non-linearities, which may significantly impact the dynamic response of the coupled device-rotorcraft system [41,42].

Friction, a highly non-linear phenomenon [43], can have significant effects on the dynamical response [44]. Hence, its identification mostly relies on experiments, especially in complex systems. In the proposed inerter system, friction can be identified at low speeds by harmonically exciting the system at low frequencies, where inertial effects are negligible and frictional forces dominate the response of the inerter [24]. For this purpose, the tuning inertias were removed from the inerter to minimise the inertia, the actuator was given a sinusoidal input signal at frequencies below 1 Hz, and the output of the load cell was recorded. One period of the recorded data was isolated, as the response is notably

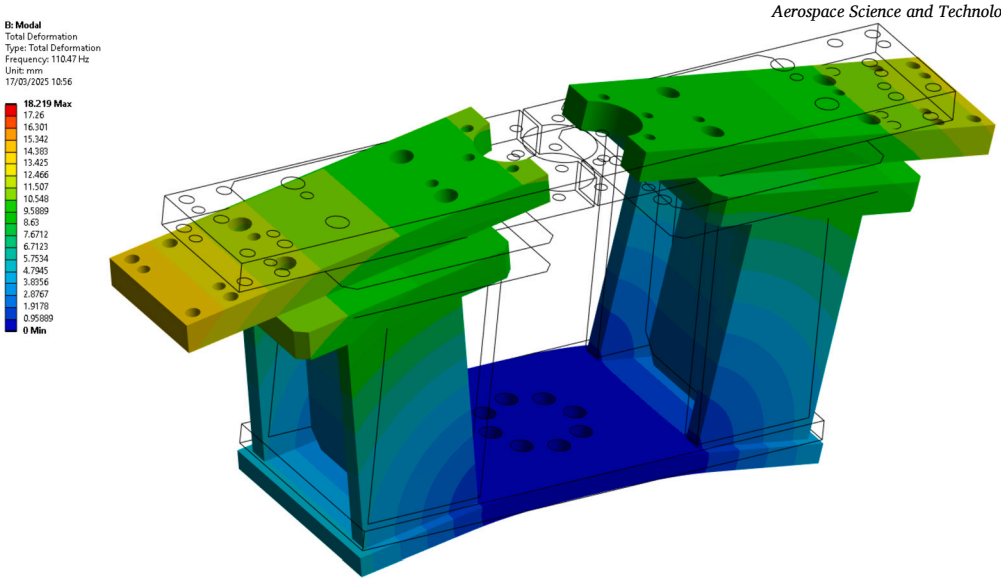

Fig. 7. First mode shape of the frame, 110 Hz. (For interpretation of the colours in the figure(s), the reader is referred to the web version of this article.)

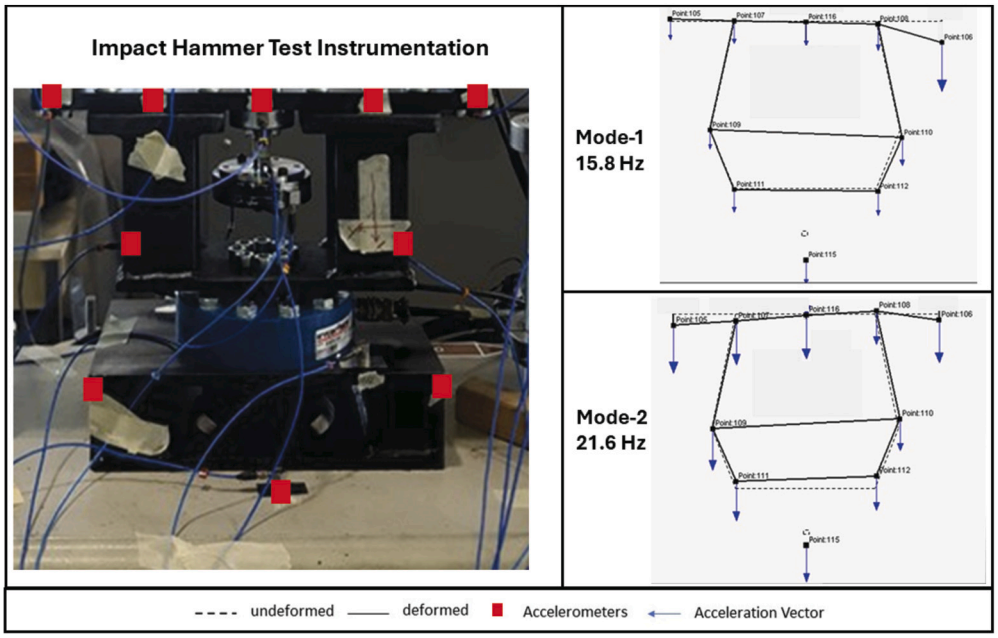

Fig. 8. Hammer tests showing the first two modes of the whole rig including the actuator.

periodic (and symmetric). A "sign" function was fitted over the signal to extract an average friction force amplitude, as shown in Fig. 9a. The friction characteristics as a function of the excitation frequency were identified at amplitudes between 0.1 mm and 0.5 mm, with increments of 0.1 mm. As illustrated in Fig. 9b, the friction level appears to depend on the excitation amplitude, but the plots suggest that deviations take place around an average value, thus a representative single value of 500 N can be assumed, which is used in non-linear form in the numerical calculations.

After identifying the friction, the inerter was tested with tuning masses for two configurations, using two and four discs, respectively. A 0.1 mm amplitude was used to stay within the operating limits of the load cell and actuator. The measurements were compared with corresponding analytical results that included inertia and friction, formulated as

$$f = b\Delta\ddot{x} - f_f \operatorname{sign}(\Delta\dot{x}) = -b\omega^2\Delta x - f_f \operatorname{sign}(\Delta\dot{x}), \tag{5}$$

where f_f is the value of the friction-related force and the inertance b is the total inertance of all rotating masses, namely $b = b_{\text{discs}} + b_{\text{screw}}$. The screw inertance $b_{\text{screw}} = I_{\text{screw}}/P^2$ remains constant for all cases, whereas $b_{\text{discs}} = N_{\text{discs}} I_{\text{disc}}/P^2$ changes depending on N_{discs}, the number of discs.

The results are presented in Figs. 10a and 10b, respectively showing the case of two and four tuning discs, for a corresponding estimated inertance of 1030 kg and 1860 kg up to 20 Hz, after which the control of the actuator failed to achieve the target input due to the motion of the base. The experiments correlate well with the analytical model, suggesting that the roller-screw inerter concept can be utilized as a strut-mounted vibration absorber. The discrepancies in the higher frequency part of the spectrum were mainly due to control difficulties at and above 15 Hz at high forcing due to excessive inertia (especially for the 4 disc case), as the test system could not reliably accelerate the inerter. This difficulty is attributed to the vibration feedback of the rubber dampers isolating the whole actuator frame from the ground and as a result including non-

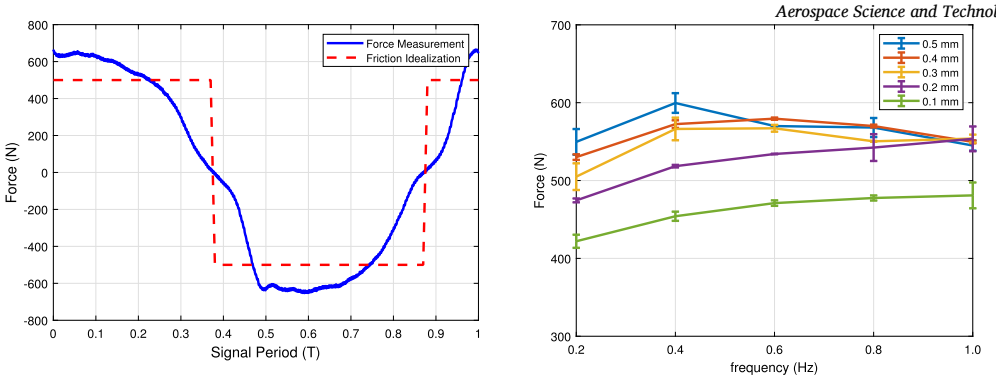

(a) Force time history at very low frequency (b) Sensitivity to prescribed motion amplitude

Fig. 9. Friction characterization at very low frequencies with error bars.

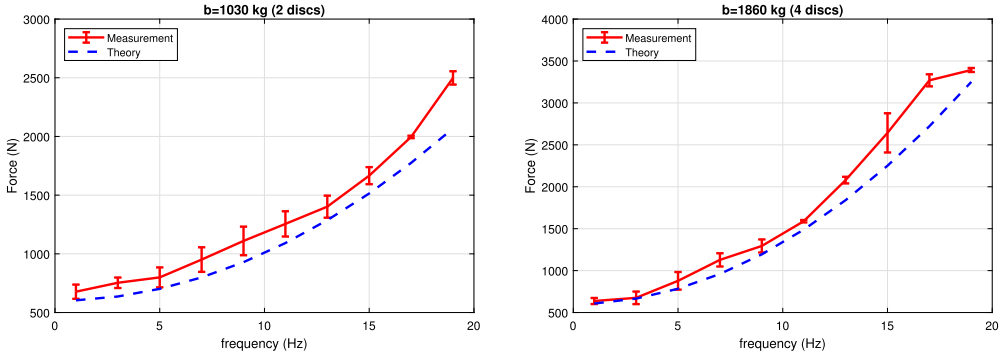

(a) 2-disc (b) 4 disc

Fig. 10. Force Measurement of 2-disc and 4-disc configurations and their comparison with theory (linear inerter+friction).

periodic and transient terms in the input. This behaviour was initially indicated in hammer test results of Fig. 8 and the rig natural frequencies are exactly the frequency range that the largest deviations between the experimental data and the numerical model are observed. However, the good correlation at frequencies lower than 15 Hz (which still refer to typical helicopter N/rev frequencies) and the acceptable overall correlation can be deemed satisfactory for demonstrating the soundness of this proof of concept.

3. Numerical analysis

In-flight demonstration of devices of this kind on a real helicopter is not viable at such an early technological readiness level. Indeed, although in principle the device is mounted in parallel with the strut and thus does not represent a primary load path for normal operations, it is expected to alter the behaviour of the gearbox-airframe connection in a significant manner, thus preliminarily requiring a careful study and a thorough validation of the concept. To this end, considering the previously postulated and estimated model and level of friction, in this Section a numerical analysis of the problem is conducted to understand the potential benefits of the inerter. A lumped-parameter quarter helicopter and a detailed helicopter model are considered, to describe the vibratory behaviour of a typical rotorcraft subjected to N/rev vibratory loads.

3.1. Lumped parameter helicopter model analysis

A simple lumped-parameter model, yet adequate to represent the dynamic operational environment of a main gearbox strut support and its companion vibration attenuation devices is the so-called "quarter helicopter" model. It consists of two masses connected by a spring, as

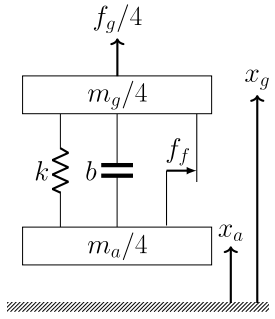

Fig. 11. Quarter H/C model.

sketched in Fig. 11. The two masses, $m_g/4$ and $m_a/4$, respectively represent the main rotor/gearbox assembly and the airframe, assuming that four identical struts, loosely parallel to the vertical axis, connect the two subsystems, idealized as perfectly rigid. Such double symmetry assumption is not usually true for helicopters but can provide a sufficiently good representation of the accelerations of airframe and gearbox when strut-mounted vibration absorbers are analysed [45]. The spring of stiffness characteristic k represents the strut. The friction identified in Fig. 9b was added as a friction element with amplitude $f_f = 500$ N. It is the only non-linear element of the otherwise linear model.

The rotor excitation, which results from the aeromechanic interaction of the rotor blades with an edgewise airflow that depends on the flight speed and on how the blades interact with their wake, is here idealized by a harmonic force $f_g \sin(N\Omega t)$ at the N/rev blade passing frequency acting on the gearbox. This is the dominant vibratory force in helicopters; its amplitude varies depending on the flight phase and speed. The N/rev force level is low in hover and manageable during

Table 1
Lumped-parameter helicopter model data.

Symbol	Definition	Value
m_g	gearbox mass (kg)	1000
m_a	airframe mass (kg)	6000
$N\Omega$	blade passage freq. (Hz)	20
k	strut stiffness (N m^{-1})	100×10^6

low speed cruise. Its amplitude increases significantly during transition from hover to cruise and in high-speed cruise. Therefore, different magnitudes of the main rotor excitation force are considered to represent various flight phases. Its value is capped at 20 kN, a realistic value for medium weight helicopters. A quarter of it is applied to our quarter helicopter model's gearbox element. Then, the equations of motion are:

$$\begin{bmatrix} \frac{m_g}{4}+b & -b \\ -b & \frac{m_a}{4}+b \end{bmatrix} \begin{Bmatrix} \ddot{x}_g \\ \ddot{x}_a \end{Bmatrix} + \begin{bmatrix} k & -k \\ -k & k \end{bmatrix} \begin{Bmatrix} x_g \\ x_a \end{Bmatrix} = \begin{Bmatrix} 1 \\ 0 \end{Bmatrix} \frac{f_g}{4} \sin(N\Omega t) + \begin{Bmatrix} -1 \\ 1 \end{Bmatrix} f_f \operatorname{sign}\left(\dot{x}_g - \dot{x}_a\right) \tag{6}$$

where f_f is the amplitude of the frequency-dependent friction contribution, whereas x_a and x_g are the vertical components of airframe and gearbox displacements. Structural damping is not considered as it would only slightly change the results, since the inerter's friction dominates energy dissipation. Data typical of medium-weight helicopters are used in the analysis [45], as reported in Table 1.

The response to a harmonic excitation of the gearbox of frequency ω and amplitude f_g, neglecting friction, is:

$$x_a = \frac{k - b\omega^2}{\frac{m_a + m_g}{4}\omega^2 \left(\left(\frac{\frac{m_g}{4}}{1+\frac{m_g}{m_a}} + b \right) \omega^2 - k \right)} \frac{f_g}{4} \tag{7}$$

For an ideal linear inerter, $b = k/\omega^2$ is thus the nominal tuning value for $\omega = N/\text{rev}$ frequency. Considering the values of Table 1, it corresponds to an equivalent inertance $b = 6.33 \times 10^3$ kg. In this case, the amplitude of the airframe acceleration exactly vanishes. Friction, and in general dissipation in the mechanism, reduces the effectiveness of the inerter; thus, some vibratory response remains.

As highlighted by Eq. (7), the problem has two poles in the origin and two imaginary conjugated poles whose frequency is smaller than but usually quite close to the tuning frequency of the system, $N\Omega$. Considering the values of Table 1, the frequency of these two poles is about 19.67 Hz, namely about 1.5% below the tuning frequency, as a consequence of the high stiffness of the strut. It is worth noticing that vibration cancellation only occurs when the rotor operates at the exact tuning frequency. Any departure will result in a loss of effectiveness of the attenuation device; an excessive reduction of the angular velocity could excite the dynamics of the structural mode resulting from the introduction of the alleviation device, actually resulting in an amplification of the vibrations. This phenomenon is well-known and affects all strut-mounted attenuation devices.

Since energy loss through friction is a non-linear phenomenon, the overall response depends on that of the vibration attenuation system, which is a function of the excitation. For this reason, the model was analysed by integrating the non-linear equations of motion in time at different forcing levels typical of helicopters. Typical time response is shown in Fig. 12, which includes:

a) the baseline configuration, without inerter,
b) the linear model with a frictionless inerter, and
c) the non-linear model, including the inerter with experimentally identified friction for a more realistic performance assessment.

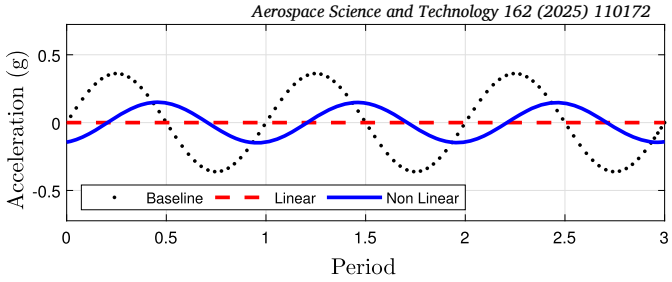

Fig. 12. An example of the fuselage response of the quarter helicopter model to harmonic excitation on gearbox mass.

The amplitudes for each case, normalized with respect to the baseline, are compared at different force levels. The friction force (averaging around 500 N) leads to a threshold effect where the friction partially masks the inertial contribution. For this reason, dissipation in the non-linear case attenuates the amplitude of the response compared to the baseline and introduces a nearly 90 deg phase delay.

The complete results are presented in Fig. 13, which shows that the benefits of the inerter increase as the forcing amplitude increases, since the fixed magnitude of the friction force, f_f, becomes less and less important than that of the excitation, f_g. This supports the idea of using an inerter for high levels of vibrational forcing, as typically happens in helicopters. Yet, it is also worth considering the sensitivity to vibration attenuation to the value of f_f, since wear, tear, and lubrication levels lead to different friction forces, which, in turn, alters inerter performance. The friction force calculations presented earlier showed a 20% uncertainty, which needs to be addressed. For this purpose, the amount of attenuation for a 20% change in friction force, i.e. $f_f = 500 \pm 100$ N, was calculated at the same hub excitation levels and presented in Fig. 14. The Figure suggests that the vibration attenuation reduces as the friction force increases, which is an expected result. The only exception happens at low-level hub excitation, where there is no attenuation at all. Additionally and more importantly, the change in vibration attenuation is on par with the change in friction level. Therefore the mild changes in friction level during the inerter operation are not expected to cause substantial changes in inerter performance.

3.2. Detailed aeroelastic model analysis

The quarter helicopter model is useful for a preliminary analysis of strut-mounted absorbers; however, the assumption of double symmetry and the lack of elastic rotor and airframe dynamics lead to an oversimplification of a real helicopter's dynamics and vibration transmissibility. To obtain a more realistic understanding of the performance of the inerter, the accurate modelling of the rotorcraft loads that excite the structure, and the correct assessment of the vibration propagation are of paramount importance in evaluating Noise, Vibration, and Harshness aspects.

The model used in the analysis is representative of a five-blade, soft in-plane main rotor, medium-weight helicopter shown in Fig. 15. It captures several aspects of the aircraft's aeromechanics:

- Flight Mechanics: the airframe's six degrees of freedom dynamics is augmented with its stability derivatives, computed through look-up tables of the fuselage, horizontal tail surface, and vertical empennage aerodynamics in CAMRAD/JA [46].
- Airframe Structural Dynamics: synthesized from a detailed NASTRAN model, comprising approximately 30 000 nodes and 17 000 elements (beams, shells, solids, rods). The airframe's elastic bending and torsion modes are extracted in the frequency range up to

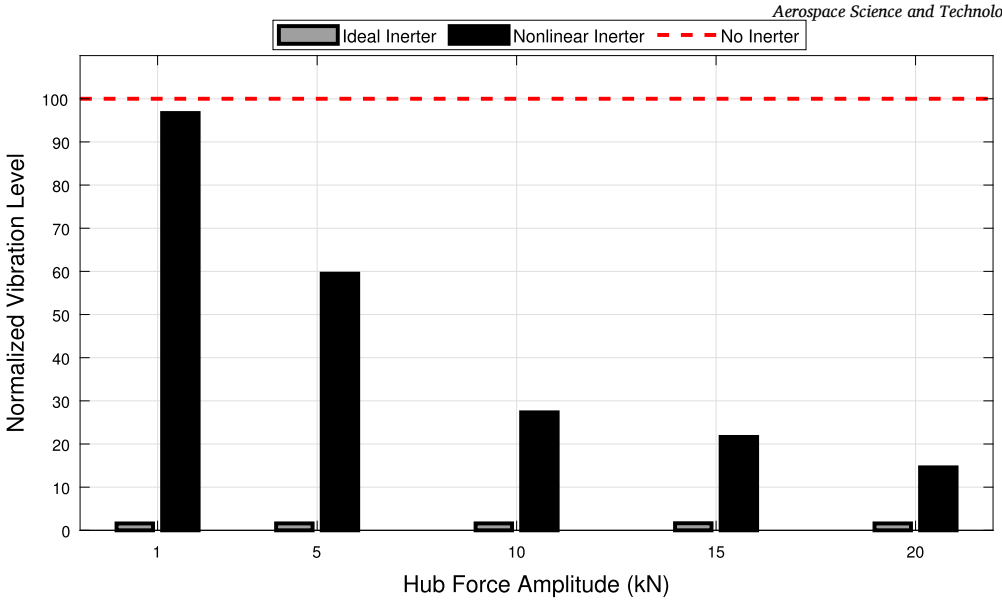

Fig. 13. Fuselage response of the quarter helicopter model to harmonic excitation on gearbox mass at different N/rev forcing amplitudes. At each forcing level, the baseline was considered as 100%, and the linear and non-linear responses were normalized using the nominal baseline value to show the reduction.

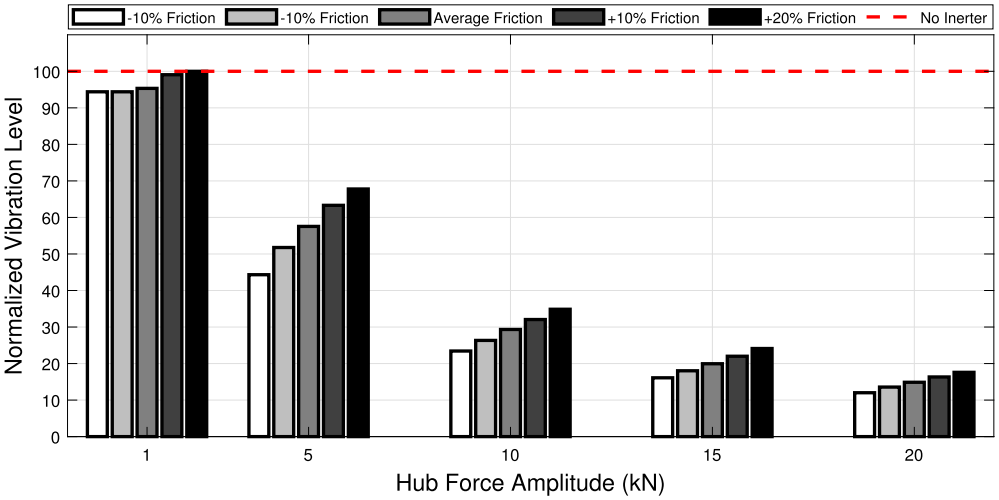

Fig. 14. Fuselage response of the quarter helicopter model to harmonic excitation on gearbox mass at different N/rev forcing amplitudes for changing friction force levels. At each forcing level, the baseline was considered as 100%, and the linear and non-linear responses were normalized using the nominal baseline value to show the reduction.

50 Hz, i.e. about twice the blade passage frequency. The struts are included in the airframe model as 1D rod elements.

- Rotors: the main and tail rotor models are formulated in CAMRAD/JA, and include the first lead-lag and up to the second flapping bending modes, as is typical for soft in-plane articulated rotors and one torsion mode associated with the compliance of the control chain. A structural damping factor of 1.5 % is assumed in the analysis, an average value for helicopter rotor blades' modal damping [1]. The rotor models are formulated in multiblade coordinates and completed by the axial state of the Pitt-Peters [47] dynamic inflow model. Inflow states only affect the low-frequency dynamics of the rotor ($\approx \Omega$) and thus are not critical when the focus is on N/rev dynamics.
- Sensors: virtual accelerometers are placed at the pilot seat locations and at the struts' connection points to support the collocation of inerters and equivalent friction dampers.
- Excitation: the N/rev vibrations (f_g) are introduced as an excitation force applied at the hub centre.
- Inerters: added to the model as 1D elements between the two terminals of the four struts as forces proportional to their relative acceleration.
- Friction: the non-linear friction force, whose amplitude of $f_f = 500$ N was determined by the experiments, is implemented for each inerter individually (inerter i), through a viscous damper that would give an equivalent energy dissipation over a cycle. The simulations start with zero damping and the damping coefficient is calculated based on the amplitude of the relative velocity ($v_{rel,i}$) of the struts using $c_{eq,i} = 4f_f/\pi v_{rel,i}$ [48] and imposed on the overall model. The iteration continues until the response converges.

The above sub-components are blended into an overall model in MASST, a Matlab-based rotorcraft aeromechanics solver [49] that uses Craig-Bampton's component mode synthesis approach [50] to combine several subsystems modelled using specialized tools like CAMRAD/JA and CAMRAD II for rotor aeromechanics and aeroelasticity, and NASTRAN for structural dynamics. More details about the model cannot be pro-

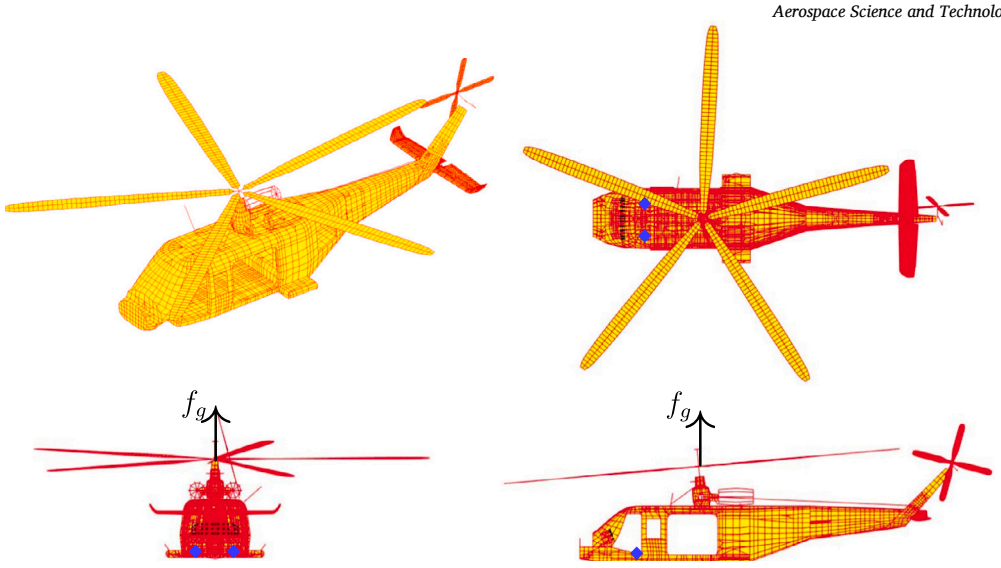

Fig. 15. Snapshot of the detailed aeroelastic model used in the analysis. Blue diamonds show the location of the pilot and co-pilot seats.

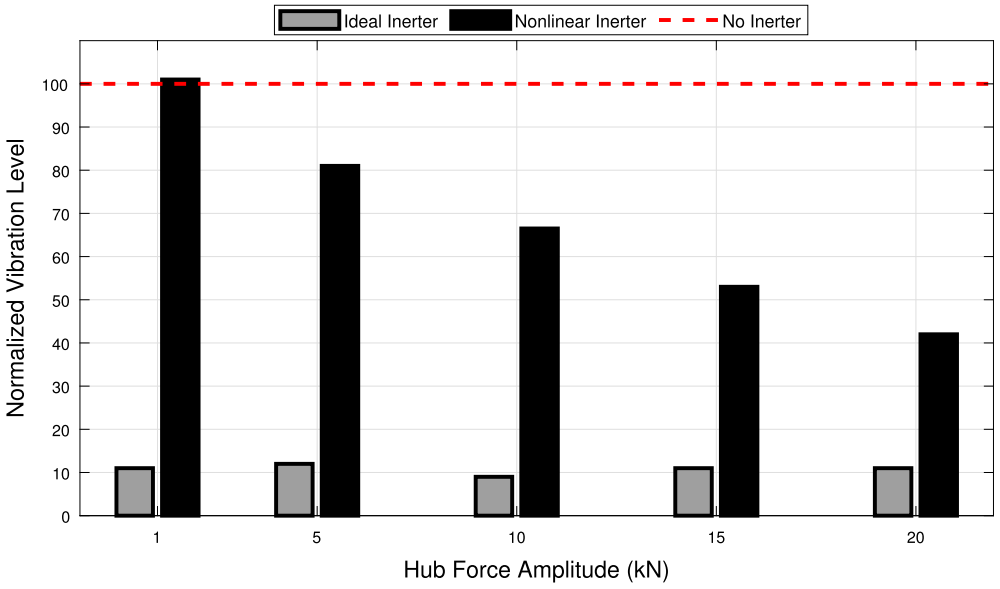

Fig. 16. Fuselage response of the detailed aeroelastic helicopter model to harmonic excitation on the gearbox mass at different N/rev forcing amplitudes. The responses of the linear and non-linear models are normalized using the baseline value.

vided due to commercial restrictions; however, they are inessential for the present discussion.

The resulting models are indicated as i) *No-Inerter*, the baseline model without inerters and related friction; ii) *Linear-Inerter*, with the inerters added to the No-inerter model but without friction; and iii) *Non-linear Inerter*, the model including the inerters and the associated friction force.

As with the quarter helicopter model, these three models were simulated to compute the accelerations at the pilot and co-pilot seats caused by the harmonic force at the hub. The results at different forcing levels are presented in Fig. 16. The same trend of increased benefit with higher forcing amplitude observed in the quarter helicopter model is also apparent in the detailed model; however, this time the residual vibration is nearly twice that obtained in the quarter helicopter case. It is worth noticing that the linear inerter model is now unable to completely cancel vibrations; a residual acceleration of about 10% of the baseline remains, as a consequence of the residual vibration transmissibility of the system.

It is worth mentioning that the amplitude of the gearbox assembly motion, x_g, is also influenced by the presence of the inerter, which in turn changes the strain in the strut due to relative elongation, which is common in strut-mounted solutions [45]. The relative motion, $\Delta x = x_g - x_a$, for a lumped mass model is:

$$\Delta x = -\frac{\dfrac{1}{1+\dfrac{m_g}{m_a}}}{\left(\dfrac{\dfrac{m_g}{4}}{1+\dfrac{m_g}{m_a}}+b\right)\omega^2-k}\frac{f_g}{4} \tag{8}$$

which, at the tuning frequency, corresponds to $-bf_g/(km_g)$. If the strut elongation after inerter installation (Δx_i) is compared to the base (only-strut) elongation Δx_0) at the tuning frequency we obtain:

Table 2
Change in N/rev strut deformation obtained using the aeroelastic helicopter model.

Configuration	Inerter Damping (%)	Relative Elongation
Base	NA	1.00
Base + Inerters	0.0	9.97
Base + Inerters	5.0	2.83

$$\left|\frac{\Delta x_i}{\Delta x_0}\right| = \left|\frac{4k}{\omega^2}\left(\frac{1}{m_g}+\frac{1}{m_a}\right)-1\right| = \left|4b\left(\frac{1}{m_g}+\frac{1}{m_a}\right)-1\right| \tag{9}$$

which shows that the inerter alters the strut elongation proportional to the strut stiffness. This, in turn, changes the strain and loads on the strut, connection elements and gear meshing.

In theory, Eq. (9) suggests that adding an inerter can reduce or increase relative strut elongation. However, main gearbox struts are typically stiff elements, designed to support static loads and maintain airframe-gearbox connection integrity. This can be verified by comparing the relative displacement in the helicopter aeroelastic model, which includes a realistic value for the stiffness of the strut. As reported in Table 2, adding a frictionless inerter increases the relative oscillatory strut elongation by almost 10 times, leading to an analogous increase of the stresses. For a higher level of friction (5%) in the inerter, the amplification reduces to approximately 3 times the nominal value, still a substantial increase. Therefore as a consequence of the inerter (or any other strut-mounted solution), the straining of the strut is amplified, and thus is the load, so it likely needs to be redesigned and the whole concept of gearbox support might need reconsideration.

3.3. Discussion

The numerical results from the quarter helicopter and the detailed aeromechanical models, considering the experimentally identified friction characteristic, showed that:

- the inerter behaves as expected and creates a force proportional to its inertance, in addition to residual friction in the system;
- the level of friction force seems to be independent of the motion amplitude. For this reason, the effectiveness of the inerter reduces at small forcing amplitudes. At greater amplitudes, the static friction force is overcome, and vibrations can be attenuated more effectively;
- at the measured friction levels, the linear inerter assumption would lead to erroneous results, with an underestimation of the residual airframe vibration response;
- the inerter was able to provide less vibration reduction when coupled to the detailed aeromechanical model;
- unlike other types of vibration alleviation devices mounted in parallel with struts, the proposed device is not affected by the need to accommodate different values of static load/stroke, as the inerter does not react to a constant or quasi-static stroke, providing a clear advantage.

This work proved that the roller-screw inerter has the potential to be a viable vibration attenuation device for helicopters. The industry is suggested to follow the below guidelines to realise their use in helicopter vibration attenuation:

- **Friction:** Although the tested device showed a reduction in the impact of friction when the level of forcing increases, friction limited its effectiveness at small forcing amplitude. Small forcing means less vibration in the cabin, yet the device should be beneficial at most if not all vibration levels and flight conditions for increased acceptance by the industry. Nevertheless, it should be emphasized that the roller screw and the bearing used in this work were not specifically designed for vibration attenuation purposes. It is expected that low-friction roller screw inerters and dedicated designs could lead to more effective vibration attenuation devices. In addition, standard procedures such as lubrication could help maintaining the device performance.
- **Airworthiness:** While strut-mounted devices can provide a global solution to cabin vibration and are not primary structural elements, their failure could have significant consequences for the struts and their attachments, ranging from increased vibrations to potential strut failure. Therefore, proposed strut-mounted inerter concept requires a thorough analysis, including laboratory and flight tests, to assess the strength, durability, and failure modes of the device and its components to meet airworthiness and certification requirements. The major risk associated with the proposed design is the potential for higher stress levels on the strut, its attachments, and the transmission system, particularly following an inerter failure. This possibility should be carefully addressed in the design of the coupled strut-inerter system.
- **Torque:** In the devised arrangement the alternate rotation of the roller and screws produces a moment of inertial nature about the axis of the device, which needs to be counteracted by an internal moment exchanged at the top. Since the usual gearbox-strut attachments are not intended to carry that moment, to use this type of device a helicopter would need to be specifically designed to withstand it. Alternatively, a solution with two identical but counter-rotating roller-screw bearings mounted in series and carrying identical inertances has been conceived and patented [51]. Since such details do not significantly affect the discussion, they are not developed further in the present work.

4. Conclusions

This work presented an in-depth experimental and numerical analysis of a novel strut-mounted inerter-based device, intended to isolate the fuselage of a helicopter from the excitation originating at the main rotor. The unique advantage of the concept is being compact and enclosing the main load-carrying element while delivering vibration attenuation at high-frequency main rotor forcing. The rigorous simulations involving realistic device behaviour through experiments showed that the proposed device can attenuate tonal vibrations at the blade passage frequency. Even considering the detrimental effect of friction, which makes the system depart from its nominal behaviour, a substantial reduction of the vibratory loads transmitted to the cabin is observed. The strut-based inerter device has potential significant implications in rotorcraft design and operation, like a lower vibration level in the whole fuselage, less use of local vibration attenuation solutions eliminating weight penalty, improved comfort of crew and passengers, and reduced vibration-related failures.

CRediT authorship contribution statement

Aykut Tamer: Writing – original draft, Visualization, Validation, Methodology, Investigation, Formal analysis, Data curation, Conceptualization. **Pierangelo Masarati:** Writing – review & editing, Supervision, Methodology, Investigation, Funding acquisition, Conceptualization. **Michele Zilletti:** Writing – review & editing, Resources, Conceptualization. **Luigi Bottasso:** Writing – review & editing, Resources, Conceptualization.

Declaration of competing interest

The authors declare the following financial interests/personal relationships which may be considered as potential competing interests: Aykut Tamer reports financial support was provided by Leonardo SpA Helicopters. Pierangelo Masarati reports a relationship with Leonardo SpA that includes: funding grants. Aykut Tamer has patent #US11433995B2 / EP3599163B1 issued to Leonardo SpA. Pierangelo

Masarati has patent #US11433995B2 / EP3599163B1 issued to Leonardo SpA. Luigi Boottasso has patent #US11433995B2 / EP3599163B1 pending to Leonardo SpA. If there are other authors, they declare that they have no known competing financial interests or personal relationships that could have appeared to influence the work reported in this paper.

Acknowledgements

This work was funded by the Leonardo Helicopter Division.

Data availability

The data that has been used is confidential.

References

[1] W. Johnson, Rotorcraft Aeromechanics, Cambridge University Press, New York, 2013.
[2] A.R.S. Bramwell, G. Done, D. Balmford, Bramwell's Helicopter Dynamics, Butterworth-Heinemann, 2001.
[3] A. Veca, Vibration effects on helicopter reliability and maintainability, TM 73-11, NASA, 1973.
[4] G. Quaranta, A. Tamer, V. Muscarello, P. Masarati, M. Gennaretti, J. Serafini, M.M. Colella, Rotorcraft aeroelastic stability using robust analysis, CEAS Aeronaut. J. 5 (1) (2014) 29–39, https://doi.org/10.1007/s13272-013-0082-z.
[5] J.K. Ljungberg, G. Neely, Stress, subjective experience and cognitive performance during exposure to noise and vibration, J. Environ. Psychol. 27 (1) (2007) 44–54, https://doi.org/10.1016/j.jenvp.2006.12.003.
[6] M. Kubo, F. Terauchi, H. Aoki, Y. Matsuoka, An investigation into a synthetic vibration model for humans:: an investigation into a mechanical vibration human model constructed according to the relations between the physical, psychological and physiological reactions of humans exposed to vibration, Int. J. Ind. Ergon. 27 (4) (2001) 219–232, https://doi.org/10.1016/S0169-8141(00)00052-4.
[7] T. Rath, W. Fichter, A closer look at the impact of helicopter vibrations on ride quality, in: AHS 73rd Annual Forum, Forth Worth, TA, USA, 2017.
[8] A. Tamer, A. Zanoni, A. Cocco, P. Masarati, A numerical study of vibration-induced instrument reading capability degradation in helicopter pilots, CEAS Aeronaut. J. 12 (2) (2014) 427–440, https://doi.org/10.1007/s13272-021-00516-8.
[9] R.L. Bielawa, Rotary Wing Structural Dynamics and Aeroelasticity, 2nd edition, AIAA, Washington, DC, 2005.
[10] B. Glaz, P.P. Friedmann, L. Liu, Helicopter vibration reduction throughout the entire flight envelope using surrogate-based optimization, J. Am. Helicopter Soc. 54 (1) (2009) 179–192, https://doi.org/10.4050/JAHS.54.012007.
[11] A. Tamer, V. Muscarello, G. Quaranta, P. Masarati, Cabin layout optimization for vibration hazard reduction in helicopter emergency medical service, Aerospace 7 (5) (2020), https://doi.org/10.3390/aerospace7050059.
[12] A. Tamer, V. Muscarello, P. Masarati, G. Quaranta, Evaluation of vibration reduction devices for helicopter ride quality improvement, Aerosp. Sci. Technol. 95 (2019) 105456, https://doi.org/10.1016/j.ast.2019.105456.
[13] T. Krysinski, F. Malburet, Mechanical Vibrations, ISTE Ltd, 2007.
[14] R. Desjardins, W. Hooper, Rotor lsolation of the hingeless rotor BO-105 and YUH-61 helicopters, in: 2nd European Rotorcraft and Powered Lift Aircraft Forum, 1976.
[15] R. Desjardins, W. Hooper, Antiresonance rotor isolation for vibration reduction, in: American Helicopter Society 34th Annual Forum, Washington DC, 1978.
[16] D. Braun, Development of antiresonance force isolators for helicopter vibration reduction, in: 6th European Rotorcraft Forum, Bristol, UK, 1980.
[17] P. Hege, G. Genoux, The SARIB vibration absorber, in: 9th European Rotorcraft and Powered Lift Aircraft Forum, 1983.
[18] D. Halmes, LIVE liquid inertia vibration eliminator, in: American Helicopter Society 36th Annual Forum, Washington DC, 1980.
[19] D. Halwes, Total main rotor isolation system, in: American Helicopter Society Northeast Region Specialist Meeting on Helicopter Vibration, Hartford, CT, 1981.
[20] D. Halwes, Total main rotor isolation system analysis, CR NAS1-16211, NASA, 1981.
[21] M.Z.Q. Chen, C. Papageorgiou, F. Scheibe, F. Wang, M.C. Smith, The missing mechanical circuit element, IEEE Circuits Syst. Mag. 9 (1) (2009) 10–26, https://doi.org/10.1109/MCAS.2008.931738.
[22] A. Gonzalez-Buelga, I.F. Lazar, J.Z. Jiang, S.A. Neild, D.J. Inman, Assessing the effect of nonlinearities on the performance of a tuned inerter damper, Struct. Control Health Monit. 24 (3) (2017) e1879, https://doi.org/10.1002/stc.1879.
[23] C. Papageorgiou, N.E. Houghton, M.C. Smith, Experimental testing and analysis of inerter devices, J. Dyn. Syst. Meas. Control 131 (1) (2008), https://doi.org/10.1115/1.3023120.
[24] F.-C. Wang, W.-J. Su, Inerter nonlinearities and the impact on suspension control, in: 2008 American Control Conference, 2008, pp. 3245–3250.
[25] S.J. Swift, M.C. Smith, A.R. Glover, C. Papageorgiou, B. Gartner, N.E. Houghton, Design and modelling of a fluid inerter, Int. J. Control 86 (11) (2013) 2035–2051, https://doi.org/10.1080/00207179.2013.842263.
[26] H. Dogan, A. Tamer, H. Enes Salman, P. Deastra, Utilising computational fluid dynamics to investigate damping effects in fluid inerter-based vibration control devices, J. Phys. Conf. Ser. 2909 (1) (2024) 012029, https://doi.org/10.1088/1742-6596/2909/1/012029.
[27] I.F. Lazar, S.A. Neild, D.J. Wagg, Using an inerter-based device for structural vibration suppression, Earthq. Eng. Struct. Dyn. 43 (8) (2014) 1129–1147, https://doi.org/10.1002/eqe.2390.
[28] L. Marian, A. Giaralis, The tuned mass-damper-inerter for harmonic vibrations suppression, attached mass reduction, and energy harvesting, Smart Struct. Syst. 19 (6) (2017) 665–678, https://doi.org/10.12989/sss.2017.19.6.665.
[29] D. De Domenico, N. Impollonia, G. Ricciardi, Soil-dependent optimum design of a new passive vibration control system combining seismic base isolation with tuned inerter damper, Soil Dyn. Earthq. Eng. 105 (2018) 37–53, https://doi.org/10.1016/j.soildyn.2017.11.023.
[30] C. Pan, R. Zhang, Design of structure with inerter system based on stochastic response mitigation ratio, Struct. Control Health Monit. 25 (6) (2018) 1–21, https://doi.org/10.1002/stc.2169.
[31] W. Shen, A. Niyitangamahoro, Z. Feng, H. Zhu, Tuned inerter dampers for civil structures subjected to earthquake ground motions: optimum design and seismic performance, Eng. Struct. 198 (August 2019) 109470, https://doi.org/10.1016/j.engstruct.2019.109470.
[32] A. Giaralis, L. Marian, Use of inerter devices for weight reduction of tuned mass-dampers for seismic protection of multi-story building: the Tuned Mass-Damper-Interter (TMDI), in: Active and Passive Smart Structures and Integrated Systems 2016, vol. 9799, April 2016, 2016, 97991G.
[33] D.J. Smith, N.D.J.Wagg, A fluid inerter with variable inertance properties, in: EACS 2016–6th European Conference on Structural Control, vol. 199, 2016, pp. 11–13.
[34] D. De Domenico, P. Deastra, G. Ricciardi, N.D. Sims, D.J. Wagg, Novel fluid inerter based tuned mass dampers for optimised structural control of base-isolated buildings, J. Franklin Inst. 356 (14) (2019) 7626–7649, https://doi.org/10.1016/j.jfranklin.2018.11.012.
[35] P. Deastra, D. Wagg, N. Sims, M.A. Mahesa, Tuned inerter dampers with linear hysteretic damping, Earthq. Eng. Struct. Dyn. 49 (12) (2020) 1216–1235, https://doi.org/10.1002/eqe.3287.
[36] X. Fu, G. Liu, S. Ma, R. Tong, X. Li, An efficient method for the dynamic analysis of planetary roller screw mechanism, Mech. Mach. Theory 150 (2020) 103851, https://doi.org/10.1016/j.mechmachtheory.2020.103851.
[37] L. Bottasso, A. Colombo, P. Masarati, A. Tamer, G. Quaranta, Helicopter kit (EP3599164B1, US 2020/0391857 A1).
[38] A. Tamer, P. Masarati, M. Zilletti, L. Bottasso, Roller-screw inerter: a novel strut-mounted device for vibration isolation, in: 47th European Rotorcraft Forum, Glasgow, UK, 2021 (held online).
[39] ROLLVIS SA, http://www.rollvis.com, last accessed June 2024.
[40] A. Tamer, A. Zanoni, A. Cocco, P. Masarati, A generalized index for the assessment of helicopter pilot vibration exposure, Vibration 4 (1) (2021) 133–150, https://doi.org/10.3390/vibration4010012.
[41] A. Tamer, P. Masarati, Helicopter rotor aeroelastic stability evaluation using Lyapunov exponents, in: 40th European Rotorcraft Forum, Southampton, UK, 2014.
[42] A. Tamer, P. Masarati, Stability of nonlinear, time-dependent rotorcraft systems using Lyapunov characteristic exponents, J. Am. Helicopter Soc. 61 (2) (2016) 14–23, https://doi.org/10.4050/JAHS.61.022003.
[43] M. Tüfekci, Y. Sun, J. Yuan, C. Maharaj, H. Liu, J.P. Dear, L. Salles, Analytical vibration modelling and solution of bars with frictional clamps, J. Sound Vib. 577 (2024) 118307, https://doi.org/10.1016/j.jsv.2024.118307.
[44] M. Tüfekci, J.P. Dear, L. Salles, Forced vibration analysis of beams with frictional clamps, Appl. Math. Model. 128 (2024) 450–469, https://doi.org/10.1016/j.apm.2024.01.031.
[45] A. Tamer, A. Zanoni, M. Daniele, P. Masarati, Multibody analysis of the influence of strut-mounted vibration alleviation devices on rotor aeromechanics, in: 8th Asian/Australian Rotorcraft Forum, Ankara, TR, 2019.
[46] W. Johnson, CAMRAD/JA, a comprehensive analytical model of rotorcraft aerodynamics and dynamics, in: Johnson Aeronautics Version, Johnson Aeronautics, 1988.
[47] D.M. Pitt, D.A. Peters, Theoretical prediction of dynamic-inflow derivatives, Vertica 5 (1) (1981) 21–34.
[48] J.P. Bandstra, Comparison of equivalent viscous damping and nonlinear damping in discrete and continuous vibrating systems, J. Vib. Acoust. Stress Reliab. Des. 105 (3) (1983) 382–392, https://doi.org/10.1115/1.3269117.
[49] P. Masarati, V. Muscarello, G. Quaranta, Linearized aeroservoelastic analysis of rotary-wing aircraft, in: 36th European Rotorcraft Forum, Paris, France, 2010, pp. 099.1–10.
[50] R.R. Craig Jr., M.C.C. Bampton, Coupling of substructures for dynamic analysis, AIAA J. 6 (7) (1968) 1313–1319, https://doi.org/10.2514/3.4741.
[51] L. Bottasso, A. Colombo, P. Masarati, A. Tamer, G. Quaranta, Helicopter kit (EP3599163B1, US 2020/0385105 A1).